

Eley–Rideal and hot-atom reaction dynamics of H(g) with H adsorbed on Cu(111)

Stavros Caratzoulas^{a)} and Bret Jackson

Department of Chemistry, Lederle Graduate Research Center, University of Massachusetts, Amherst, Massachusetts 01003

Mats Persson

Department of Applied Physics, Chalmers University of Technology and University of Göteborg, S-412 96 Göteborg, Sweden

(Received 2 June 1997; accepted 21 July 1997)

Quasiclassical trajectory studies have been performed for the reaction between an H (or D) atom incident from the gas phase and a H (or D) atom adsorbed onto a Cu(111) surface. Results from a density functional calculation of the interaction between H and a Cu(111) surface are used to construct a detailed potential energy surface which contains all six nuclear degrees of freedom. Impacts of the incident atom close to the adsorbate can lead to direct Eley–Rideal reactions and the dynamics of these reactions are explored. Interaction of the incident atom with the adsorbate also results in trapping, with a high probability. This adsorbate-mediated trapping mechanism is important for impacts within 2 Å of the adsorbate. At larger impact parameters scattering from the corrugation also leads to trapping. These trapped ‘‘hot’’ atoms can go on to react with an adsorbed species, and the dynamics of such hot-atom reactions are explored. The final-state distributions of the products are examined with regard to isotope effects for the direct and hot-atom pathways, and compared with experiment. © 1997 American Institute of Physics. [S0021-9606(97)02640-8]

I. INTRODUCTION

Many of the reactions that take place on catalytic surfaces occur via the Langmuir–Hinshelwood (LH) mechanism, in which the reactants are initially adsorbed onto the surface and in thermal equilibrium with the substrate. A less common pathway is the Eley–Rideal (ER) mechanism, in which a gas-phase species reacts directly with an adsorbed species. Substantial experimental evidence for these ER reactions has appeared in recent years (see Refs. 1–17). A common experimental signature of an ER reaction is a large exothermicity, which shows up in the translational and internal energy of the products. For instance, the LH recombination $\text{H}(\text{ads}) + \text{H}(\text{ads}) \rightarrow \text{H}_2(\text{g})$ is nearly thermoneutral on most transition metals, because the H–metal bond is typically around 2.4 eV and the H–H bond energy is about 4.7 eV. The ER reaction $\text{H}(\text{g}) + \text{H}(\text{ads}) \rightarrow \text{H}_2(\text{g})$, on the other hand, is exothermic by about 2.3 eV. Another signature of ER reactions is that they should exhibit some sensitivity to the initial conditions of the incident species. While most of these experimental studies involve ER reactions on transition metal surfaces, there have been several studies on semiconductors,^{9–12} where H-atom beams are used to hydrogenate Si surfaces or to remove halogen atoms from Si or Ge.

The most detailed experimental studies are of H(g) reacting with either Cl adsorbed onto Au(111),^{3,6,7} or H adsorbed onto Cu(111).^{5,8} For these systems, rotational, vibrational, and translational distributions were measured for the product molecules. We have examined these reactions theo-

retically in some detail, using both quantum and classical methods.^{18–23} For both reactions we found that the direct pathway, where the incident H does not adsorb onto the surface before reacting, was feasible. The surface temperature dependence of the $\text{H}(\text{g}) + \text{Cl}(\text{ads})$ reaction was explained in terms of an increased reactivity as the adsorbate became vibrationally excited.¹⁹ Several fully quantum calculations were implemented for the $\text{H}(\text{g}) + \text{H}(\text{ads})$ reaction, using a flat-surface model in which the effects of corrugation were ignored for the relatively smooth Cu(111) surface. Reaction cross sections and product rovibrational and translational distributions were computed for various isotopic combinations of H and D.^{21–23} Reasonable agreement was found with the experiments of Rettner and Auerbach⁸ for the distribution of the exothermicity among the product degrees of freedom.

However, there are several questions that remain to be answered. Our computed cross sections were typically about an order of magnitude smaller than the 5 \AA^2 measured in the experiments.⁸ This discrepancy suggests that other pathways to reaction may be important, or that our calculation has significant errors arising from the neglect of corrugation or an inadequate potential energy surface (PES). Many alternate reaction pathways exist. In our flat-surface studies²² we found a large cross section of about 18 \AA^2 for adsorbate-mediated trapping, in which the incident particle scatters from the adsorbate, transferring enough of its translational energy normal to the surface to other degrees of freedom to become trapped. The resulting ‘‘hot’’ atom travels rapidly across the surface, and should have a significant probability of reacting with another adsorbate,²⁴ particularly at the high surface coverages used in the experiments. These hot atoms, while bound normal to the surface, can be 2 eV or more

^{a)}Present address: Department of Chemistry, University of Birmingham, Birmingham B15 2TT, United Kingdom.

above the ground state. If they react before dissipating this excess energy into the substrate, the resulting large exothermicity shows up in the desorbing products. Such reactions may be difficult to distinguish from those resulting from a direct encounter from the gas phase and both are often referred to as ER. As in our previous studies, however, we will only apply the term ER to direct reactions in which the incident atom does not trap onto the surface. The corrugation can play an important role by modifying the dynamics of direct reactions and by providing a mechanism for trapping the incident atom into (and scattering them out of) trapped hot-atom states.

In this paper, we address the above questions in a model that incorporates surface corrugation effects. These effects are included in an improved PES constructed using recent results of density functional calculations of the total energy for the H–Cu(111) interaction.²⁵ Because all six degrees of freedom are included, a quantum calculation is not possible and quasiclassical methods are used. However, we have made detailed comparisons between quantum and quasiclassical results for our flat-surface model and have thus “bench marked” the quasiclassical dynamics for this system, to some extent.^{20–22} Because there are no barriers and the reaction involves high energies, the quasiclassical results reproduce the essential features of the reaction in a qualitative (and sometimes semiquantitative) fashion. We examine the dynamics of these reactions and compute detailed product state distributions. We also examine the propensity to form hot atoms by scattering from either the adsorbate or the corrugation. We then explore the reaction of the corrugation-mediated trapped atoms with the adsorbate and compare the product state distributions with those from the direct reaction. Finally, we investigate the relationship between the opacity and the product rovibrational distribution, an idea explored in our earlier flat-surface work and an important concept in gas-phase scattering. In Sec. II, we review our flat-surface results and ideas. In Sec. III, our current model and PES calculations are described. The results are presented and discussed in Sec. IV and we conclude with a brief summary in Sec. V.

II. FLAT SURFACE RESULTS

Here we review the results of our flat-surface model, a complete description of which can be found in the literature.^{20,22} The PES for two bodies over a flat surface can be described by three degrees of freedom: z_i and z_t , the distance of the incident (gas phase) and target (adsorbed) atoms above the plane of the surface, respectively, and ρ , the lateral separation of the two bodies in the plane of the surface (see inset of Fig. 1). The momenta conjugate to the remaining three degrees of freedom are conserved, reducing the dimensionality of the problem from six to three. Using a model LEPS (London–Eyring–Polanyi–Sato) potential, fitted to experimental data and theoretical calculations, we implemented quasiclassical (QC) and fully quantum studies of the reaction of gas-phase H or D with H or D adsorbed onto Cu(111). In the quantum calculation,²⁰ the wave func-

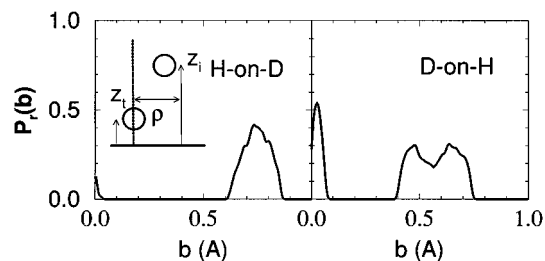


FIG. 1. Quasiclassical reaction probabilities, $P_r(b)$, as a function of impact parameter b , for H-on-D and D-on-H. The inset depicts the scattering geometry in the flat-surface model, together with the coordinates of the incident and target atoms.

tion was represented on a large three-dimensional grid, and well-known pseudospectral techniques were used to evolve it in time. A projection-operator correlation-function approach was used to extract the rovibrational distributions from the scattered product wave function. The quasiclassical calculations were implemented in the usual fashion, with the proper zero-point energies included in the initial conditions. The quasiclassical reaction cross section is written

$$\sigma_r = 2\pi \int_0^\infty P_r(b) b db, \quad (1)$$

where the opacity function $P_r(b)$ is the fraction of trajectories at each initial impact parameter, $b = \rho(t \rightarrow -\infty)$, which are reactive.

In gas-phase scattering theory,²⁶ the opacity function is often related to the internal state distribution of the products. For example, for a given incident momentum the impact parameter defines the angular momentum of the “collision complex,” which can be mapped onto the rotational state of the resulting product. Similarly, one might argue that reactive impacts near the product equilibrium bond length lead to products in the vibrational ground state, while impacts away from this lead to compressed or stretched (i.e., vibrationally excited) product molecules. Although these simple but physical ideas have been applied to surface reactions, their validity or utility is not clear because the presence of the surface can change the dynamics considerably. In Fig. 1 we plot the quasiclassical opacity functions for the case of H-on-D [i.e., H(g) incident on D(ads)] and D-on-H. All results are for an incident kinetic energy of 0.075 eV. The opacity functions are similar in that there is some reactivity near $b = 0$, with most of the reactive trajectories having impact parameters within a few tenths of an Å of the equilibrium bond length, $r_0 = 0.741$ Å. Because of the area element in Eq. (1), the collisions at small b contribute little to the total cross section. All isotopic combinations share the unusual “hole” in the opacity function for impacts less than about 0.5 Å. This is significantly different from gas-phase opacity functions, which are typically assumed to be roughly constant for b between zero and some maximum value. Be-

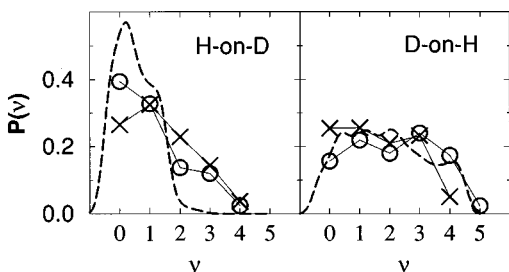


FIG. 2. Comparison between the calculated and measured vibrational distributions, $P(\nu)$, for H-on-D and D-on-H. The quantum mechanical and quasiclassical results are depicted by the circles and the dashed lines, respectively. The experimental data, taken from Ref. 8, are depicted by crosses.

cause $P_r(b)$ differs for the various isotopic combinations, one would expect that the product state distributions would also differ.

In Fig. 2 and Table I we present calculated^{21,22} and experimental⁸ results for three isotopic combinations. The QC results are in reasonable agreement with those from the quantum calculation for the cross sections and the average center-of-mass and internal energies. The agreement is not as good for the average product rotational and vibrational quantum numbers, $\langle j \rangle$ and $\langle \nu \rangle$, respectively, and the HD vibrational and rotational (not shown) distributions. The QC calculation tends to overestimate rotational excitation and underestimate vibrational excitation, showing the largest errors for the H-on-D combination. However, the general trends are reproduced. The agreement between theory and experiment is also reasonable, except for the reaction cross sections, which are considerably larger in the experiments. The distribution of energy in the internal and translational product degrees of freedom and the trends with isotope are roughly consistent with experiment. In particular, the product vibrational distributions are in good agreement with experiment for the two isotopic combinations shown in Fig. 2. Note also that the product state distributions are correlated to some extent with the opacity functions in Fig. 1. Most of the reactive collisions for H-on-D occur near r_0 , leading to little vibrational excitation of the product HD. For D-on-H, on the other hand, most reactive collisions occur for $b < r_0$, and the products are highly vibrationally excited. One would also expect less rotational excitation for D-on-H, and this is also seen, although the isotopic trends in the experiment are not as strong.

In order to better understand the dynamical origins of the

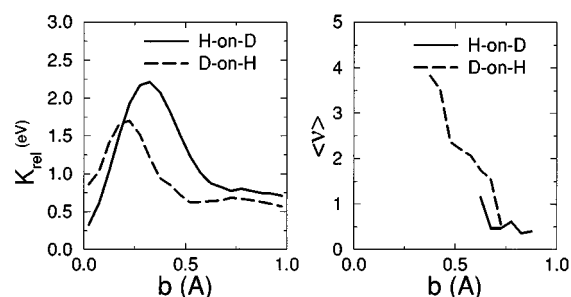


FIG. 3. Quasiclassical averages of the relative kinetic energy along the surface, K_{rel} , and vibrational quantum number $\langle \nu \rangle$, as a function of impact parameter b .

isotope effects, the hole in the opacity function, and the connection between the opacity and the product distributions, we plot in Fig. 3 K_{rel} as a function of the impact parameter, where K_{rel} is the relative lateral kinetic energy of the two particles following a collision which leads to trapping of the incident atom. As discussed in an earlier paper,²² the large acceleration of the incident atom and the similar masses of the two particles lead to very efficient energy transfer and a large trapping cross section. At small b the relative kinetic energy of the particles parallel to the surface can be quite large. Thus for small impact parameters, the particles may be too far apart (or have too much K_{rel}) to react by the time they have recoiled from the surface. Comparison with Fig. 1 suggests that this adsorbate-mediated trapping mechanism may cause the hole in the opacity function. As b increases, this energy transfer becomes less efficient and reactions appear to occur when K_{rel} drops below about one eV. Because H is more strongly deflected from D than D is from H, a larger impact parameter is required for reaction, leading to the opacity functions in Fig. 1. In Fig. 3, we also plot $\langle \nu \rangle$ as a function of impact parameter, and it seems to be fully consistent with the opacity arguments made earlier. Note, however, that $\langle \nu \rangle$ also scales closely with K_{rel} suggesting that this relative kinetic energy maps directly onto product vibration, an attractive idea. We have also examined $\langle j \rangle$ as a function of b and found almost no correlation; that is, almost any impact parameter can lead to any final rotational energy. This finding is perhaps not surprising, since the presence of the surface eliminates conservation of angular momentum, and the reactive trajectories can be quite complicated. In Sec. IV we see to what extent these ideas are retained on a corrugated surface.

TABLE I. Quantum mechanical and quasiclassical flat-surface results for the reaction cross section, σ_r , the average product internal energy, $\langle E_{\text{int}} \rangle$, and average product vibrational and rotational quantum numbers $\langle \nu \rangle$ and $\langle j \rangle$, respectively. The results in parentheses are from the quasiclassical calculations.

		σ_r (\AA^2)	$\langle E_{\text{int}} \rangle$ (eV)	$\langle \nu \rangle$	$\langle j \rangle$
H-on-H	theory	0.46 (0.42)	1.54 (1.44)	1.34 (1.37)	8.1 (8.7)
H-on-D	theory	0.27 (0.31)	1.48 (1.48)	1.05 (0.51)	11.2 (14.5)
H-on-D	expts	≈ 5	1.2	1.4	7.3
D-on-H	theory	0.39 (0.30)	1.67 (1.69)	2.13 (1.89)	8.8 (11.7)
D-on-H	expts	≈ 5	1.3	1.6	7.0

III. THEORY

The density functional calculations of Strömqvist and co-workers²⁵ are used to construct a six degree-of-freedom PES describing the interaction between two hydrogen atoms on a Cu(111) surface. Quasiclassical methods are used to study the direct ER and hot-atom reactions between a gas-phase H and an H adsorbed in the threefold hollow site of Cu(111). The metal surface is assumed to be corrugated but rigid; that is, no lattice vibrations are considered. We think that the lattice phonons have some effect on the dynamics, but not a dominant one, because of the small gas-to-surface atom mass ratio and the efficiency of the H–H energy transfer. The minor role of the substrate phonons is supported by classical trajectory studies of the adsorption of a single H atom on Cu(111),²⁵ which showed that trapping in the initial collision with the surface is dominated by the surface corrugation.

A. Density functional calculations

The details of the first principle total-energy calculations for a single H atom on Cu(111) have been reported elsewhere.²⁵ For easy reference, we shall just present the main ingredients and results of these calculations.

The calculations were performed in density functional theory using the generalized gradient approximation for the exchange correlation energy. The total energy was computed in a super-cell geometry using a plane-wave and pseudopotential code. The Cu(111) surface was represented in the super cell by a slab of four atomic layers with three substrate atoms in each layer. The cell contained a single H atom, which corresponds to a coverage of 1/3 and a large H–H distance of about 4.4 Å. All valence electrons of the Cu atom are included. To obtain the proper energy of the isolated Cu(111) slab and H atom, we performed a spin-polarized calculation of the isolated H atom. In Table II, we have listed

TABLE II. First principle values for binding parameters of H on Cu(111) taken from Ref. 25. D is the potential energy minimum located at $z^{(0)}$, and $\hbar\omega$ is the calculated vibrational energy for the H atom normal to the surface.

Site	D (eV)	$z^{(0)}$ (Å)	ω (meV)
Atop	1.93	1.53	217
Bridge	2.31	1.08	139
Hollow	2.46	0.954	144

the calculated binding parameters that we use to construct our PES.

The calculated binding parameters are in good agreement with available experimental data. The H atom prefers to adsorb in a hollow site with a slight preference of about 5 meV for the fcc configuration, that is, the configuration where there is no underlying substrate atom in the second layer. The calculated well depth of about 2.37 eV is in good agreement with the measured well depth of about 2.4 to 2.5 eV when correcting for the zero-point energy of about 0.16 eV, as estimated from measured vibrational frequencies.²⁷ The calculated vibrational energy in the harmonic approximation of about 145 meV is about 10% larger than the measured vibrational energy of about 129 meV by Lamont and co-workers.²⁸ Mattson and co-workers²⁹ have demonstrated that multidimensional anharmonic effects may decrease this vibrational excitation energy by about 15%.

B. Model PES

The positions of the incident and target (initially adsorbed) atom are given by the vectors \mathbf{r}_i and \mathbf{r}_t , respectively. Henceforth, the subscripts “ i ” and “ t ” will refer to these atoms. The x and y components of these vectors lie in the surface plane, and the z component is perpendicular to the surface. The relative position vector of the two atoms is $\mathbf{r} = \mathbf{r}_t - \mathbf{r}_i$. In this electronically adiabatic study the reaction dynamics take place on a single PES, for which we use the following LEPS form:

$$V(\mathbf{r}_i, \mathbf{r}_t) = U_i(\mathbf{r}_i) + U_t(\mathbf{r}_t) + U_m(r) - \sqrt{Q_m(r)^2 + [Q_i(\mathbf{r}_i) + Q_t(\mathbf{r}_t)]^2} - Q_m(r)[Q_i(\mathbf{r}_i) + Q_t(\mathbf{r}_t)]. \quad (2)$$

U_j and Q_j , where $j = t, i, m$, are associated with the single atom-surface interaction ($i = t, i$) and the H–H molecular interaction ($i = m$). They have the usual forms:

$$U_j = \frac{D_j}{4(1 + \Delta_j)} [(3 + \Delta_j)\exp(-2\alpha_j(w_j - w_j^{(0)})) - (2 + 6\Delta_j)\exp(-\alpha_j(w_j - w_j^{(0)}))], \quad (3)$$

$$Q_j = \frac{D_j}{4(1 + \Delta_j)} [(1 + 3\Delta_j)\exp(-2\alpha_j(w_j - w_j^{(0)})) + (6 + 2\Delta_j)\exp(-\alpha_j(w_j - w_j^{(0)}))]. \quad (4)$$

For the H–H interaction, U_m and Q_m are only functions of

the interatomic separation, $w_m = r$, and thus the corresponding well depth, D_m , and equilibrium position, $w_m^{(0)} = r_0$, are constants. The standard values $D_m = 4.745$ eV, $\alpha_m = 1.943$ Å⁻¹, and $r_0 = 0.741$ Å fit to both theoretical and experimental data, are used.

For the atom-surface interactions ($j = t, i$), $w_j = z_j$, the well depths D_j and the equilibrium positions $w_j^{(0)}$ vary across the corrugated metal surface. We write, for $j = t, i$:

$$D_j(x_j, y_j) = D_0(1 - \epsilon B(x_j, y_j)), \quad (5)$$

$$w_j^{(0)}(x_j, y_j) = z_0(1 + \delta B'(x_j, y_j)). \quad (6)$$

Given the origin at an atop site and the symmetry of the Cu(111) surface, $B(x, y)$ has the general form

TABLE III. Fourier coefficients for the corrugation function defined in Eq. (7). Unprimed coefficients refer to the corrugation function for the well depth and the primed coefficients refer to the corrugation function for the equilibrium position.

Coefficients	$B(x,y)$	$B'(x,y)$
a_{00}	1.7739	1.4442
a_{01}, b_{11}	0.4797	0.4977
a_{11}, b_{12}	-0.0918	-0.05
a_{02}, b_{22}	0.0273	0.0116
a_{12}, b_{13}, b_{23}	0.0043	0.0007
a_{03}, b_{33}	-0.0025	-
a_{22}, b_{24}	-0.0004	-

$$\begin{aligned}
 B(x,y) = & \frac{a_{00}}{2} + \sum_{m=1}^{\infty} a_{mm} \cos(2m\alpha x) \\
 & + \sum_{m=1}^{\infty} b_{mm} \cos(2m\beta y) \\
 & + 2 \sum_{m=0}^{\infty} \sum_{n>m}^{\infty} a_{mn} \cos[(m+n)\alpha x] \cos[(m-n)\beta y] \\
 & + 2 \sum_{m=1}^{\infty} \sum_{n>m}^{\infty} b_{mn} \\
 & \times \cos[(m-n)\alpha x] \cos[(m+n)\beta y], \quad (7)
 \end{aligned}$$

where $\alpha = 2\pi/c$, $\beta = 2\pi/c\sqrt{3}$, and $c = 2.55 \text{ \AA}$ for Cu(111); a similar expression holds for $B'(x,y)$. The parameters D_0 and ϵ in Eq. (5) and the Fourier coefficients in Eq. (7) were determined in the following way. A ‘local’ corrugation function was constructed by placing Gaussian functions at the atop and the threefold hollow sites of the surface, covering an area extending over several surface unit cells. The amplitudes and widths of these Gaussians were fitted to our first principle total energy calculations at the atop, bridge, and threefold hollow sites. This ‘local’ corrugation function was then numerically Fourier transformed, according to Eq. (7), to obtain the Fourier coefficients a_{mn} and b_{mn} . Only coefficients of $\mathcal{O}(10^{-4})$ or larger were retained. The same procedure was used to determine z_0 , δ , and the Fourier coefficients a'_{mn} and b'_{mn} defining $B'(x,y)$. The coefficients retained in the truncated Fourier expansions are given in Table III, and all of the remaining potential parameters are given in Table IV.

The parameters α_j ($j=t,i$) for the H–Cu interactions have not been allowed to vary across the surface. They were

set equal to the value used in our previous flat-surface studies,²² where they were fitted, within the harmonic approximation, to the first principle value of the H–Cu vibrational frequency at the hollow site. The values for the Δ_j were also taken from these studies, where they were chosen to reproduce the barrier for the dissociation of H_2 on Cu(111), which has been well studied by both experiment and theory.^{30,31} This allows us to more easily compare our results with the flat-surface studies since only the corrugation part of the PES is different. For $\alpha_j = 1.0$ we obtain the harmonic frequencies 127.5, 139, and 144 meV at the atop, bridge, and hollow sites, respectively. These are in excellent agreement with the theoretical values, listed in Table II, for the hollow and bridge sites, which are the most important for motion on the surface. The resulting frequency for lateral motion along either x or y in the hollow site, in the harmonic approximation, is 85 meV.

C. Calculations

We perform quasiclassical calculations for the motion of the two hydrogen atoms; one initially adsorbed in a threefold hollow site and one incident from the gas phase. With the term quasiclassical, we stress that the zero-point energy of the target atom is accounted for in its motion both normal and parallel to the surface. Because we wish to treat all six molecular degrees of freedom, a quantum approach is not possible. However, as discussed in the previous section, the reaction has no barrier and is strongly exothermic, and the quasiclassical method has given results in reasonable qualitative agreement with quantum calculation. We integrate Hamilton’s equations of motion in Cartesian coordinates.

For the adsorbed atom, motion in the three coordinate directions is nearly independent at low energies, and the initial conditions are sampled at random at a given vibrational energy level using the classical periodic orbits at this energy, for each coordinate. The adsorbed H is initially in its ground vibrational state, with a zero-point vibrational energy of 71 meV in the z direction, and 42.5 meV in the x and y directions. The trajectory for the incident atom is started 7 \AA above the surface. Only normal incidence is considered and we give the atom an initial translational energy $E_i = 75$ meV. Because of the large energy release in the adsorption and in the reaction, the results were found to vary weakly with the incident energy in earlier studies.^{20,22} The initial lateral coordinates x_i and y_i are sampled uniformly within a domain extending over several unit cells.

The classical trajectories are classified as reacted, reflected, or trapped. We do not observe any exchange processes. Reaction to form H_2 or reflection of the incident H atom are easily defined, while the definition of trapping is somewhat arbitrary. We use the term ‘trapping’ and not ‘sticking’ since in the calculation the trapped atoms cannot dissipate their excess energy into the substrate, eventually relaxing to the ground state. In most cases, the incident atoms that become trapped have enough kinetic energy parallel to the surface to travel rapidly across the surface. When, however, the condition $r \geq 25 \text{ \AA}$ is satisfied, and both atoms

TABLE IV. LEPS potential parameters.

H–H	H–Cu(111)
$D_m = 4.745 \text{ eV}$	$D_0 = 2.4213 \text{ eV}$
$\alpha_m = 1.943 \text{ \AA}^{-1}$	$\alpha_t = \alpha_i = 1.0 \text{ \AA}^{-1}$
$r_0 = 0.745 \text{ \AA}$	$z_0 = 1.0022 \text{ \AA}$
$\Delta_m = -0.2$	$\Delta_t = \Delta_i = 0.2$
	$\epsilon = 0.0944$
	$\delta = 0.2508$

are bound to the surface, we arbitrarily terminate the trajectory and label it as trapped, even though these trajectories, if given sufficient time, may eventually become reactive or reflected. One of the reasons that we sample such a large surface area with $x_i(0)$ and $y_i(0)$ is that we want to explore hot-atom reactions in which the incident atom scatters from the corrugation and becomes trapped before encountering an adsorbate. The product molecules are assigned a rotational “quantum number” $j=J/\hbar$, where J is the classical angular momentum of the molecule. As before, we also extract a vibrational “quantum number,” ν , which is computed via semiclassical quantization.²⁰ Continuous distributions for all the observable quantities are obtained by introducing a small finite resolution via a Gaussian resolution function.

For the flat-surface studies at normal incidence, the presence of azimuthal symmetry allowed us to define an opacity as a function of impact parameter. For our corrugated surface this is not possible and we define our cross section by

$$\sigma_{\mathbf{r}} = \int \int_{\mathcal{D}} P_{\mathbf{r}}(x_i, y_i) dx_i dy_i, \quad (8)$$

where the double integration is over the domain \mathcal{D} sampled by the initial coordinates of the incident atom. Our two-dimensional opacity function $P_{\mathbf{r}}(x_i, y_i)$ is the fraction of trajectories which react for a given x_i and y_i . To facilitate a connection with the flat surface studies and to simplify our description of behavior as a function of surface impact site, we will often refer to the one-dimensional impact parameter $\rho_0 = \sqrt{x_i(0)^2 + [y_i(0) - c/\sqrt{3}]^2}$. At normal incidence this parameter is the initial lateral distance of the incident atom from the threefold hollow site of the target atom and does not account for the initial lateral displacement of the target atom. We also make use of the one-dimensional reactivity function, $R(\rho_0)$, where $R(\rho_0)d\rho_0$ is the relative number of reactive trajectories in the interval ρ_0 to $\rho_0 + d\rho_0$, normalized so that $\int_0^\infty R(\rho_0)d\rho_0 = 1$. Thus R is proportional to the opacity function $P_{\mathbf{r}}(x_i, y_i)$ averaged over all x_i and y_i for a given ρ_0 , times ρ_0 .

IV. RESULTS AND DISCUSSION

A. Reaction and trapping

The reactivity, $R(\rho_0)$, and two-dimensional opacity, $P_{\mathbf{r}}(x_i(0), y_i(0))$, defined above, are plotted in Figs. 4 and 5, respectively, for H-on-H. The opacity is plotted as scattered points marking the initial values of x_i and y_i for trajectories leading to reaction. The corrugation leads to a great deal of structure and we can think of the reactivity as arising from three distinct regions. The first region corresponds to $\rho_0 \leq 1.2 \text{ \AA}$, which accounts for $\approx 50\%$ of the total reaction cross section, $\sigma_{\mathbf{r}} = 0.57 \text{ \AA}^2$. Most of this reactivity occurs in a “ring” of radius 0.3 \AA about the adsorbate and corresponds to direct ER processes. Direct ER reactions also occur for trajectories incident in the hollow-to-bridge region. The reactive trajectories in this first region all have very short reaction times (see below) and the turning points of the incident particles cluster in a ring of radius $\approx 0.9 \text{ \AA}$ about the adsorbate. The second region, corresponding to the peak at

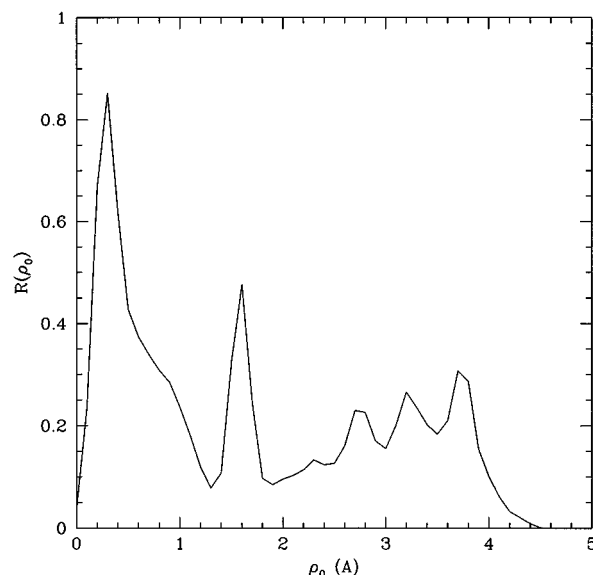


FIG. 4. Relative reactivity R as a function of the impact parameter ρ_0 .

$\rho_0 = 1.6 \text{ \AA}$ in Fig. 4, results from trajectories which are incident on the “far” sides of the three hollow sites nearest the target atom. “Far” refers to the side opposite to the bridge region connecting these hollow sites to the adsorbate hollow. These trajectories deflect from the Cu atom on the far side of these hollow sites, travelling rapidly across the bridge region towards the adsorbate, and reacting with it. In the third region, $\rho_0 \geq 2.0 \text{ \AA}$, the distribution of reactive trajectories is diffuse. This region corresponds to incident particles which also scatter from the corrugation into trapped states, eventually finding and reacting with the adsorbate. This trapping mechanism, often referred to as diffraction-mediated selec-

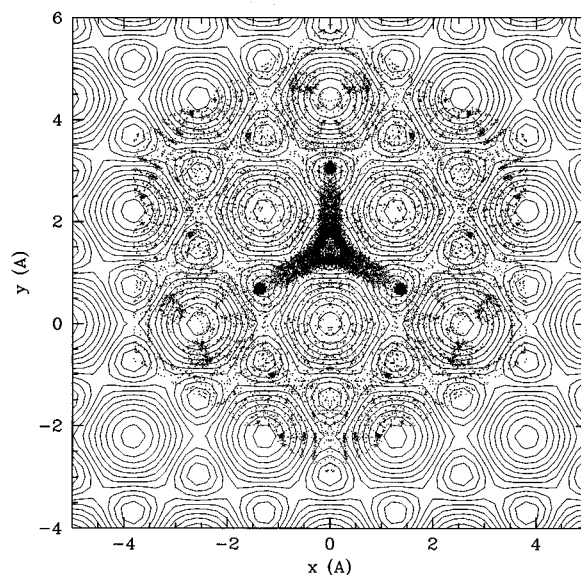


FIG. 5. Two-dimensional “opacity function,” $P_{\mathbf{r}}(x_i, y_i)$, for reactive trajectories, plotted as scattered points marking the initial values of x_i and y_i . The contours shown are for the corrugation function of the surface. The adsorbate hollow site is at $x=0 \text{ \AA}$ and $y=1.47 \text{ \AA}$.

tive adsorption (DMSA), creates the hot atoms that are responsible for the reactivity at large ρ_0 . Because we do not treat the particle translation quantum mechanically, we do not have diffraction *per se* and do not get DMSA resonances. However, at the large scattering energies of this reaction, there are many diffraction channels open and classical mechanics should give reasonable results. In this work we will use the terms adsorbate-mediated and corrugation-mediated trapping, although the two mechanisms are often difficult to disentangle.

The corrugation is responsible for several interesting effects. In the flat-surface studies, the competition between reaction and adsorbate-mediated trapping lead to a low reaction cross section and a hole in the opacity function. For the corrugated surface, however, there is a caging effect wherein the Cu atoms around the adsorbate keep the incident and target atoms from moving away from each other too rapidly. The result is a much smaller ‘‘hole,’’ with a radius of only $\approx 0.2 \text{ \AA}$, as can be seen most clearly in Fig. 5. However, the addition of corrugation adds an additional trapping mechanism which both adds to and competes with reaction. For impact sites of the incident atom more than a few tenths of an \AA away from the reactive hollow or bridge regions near the adsorbate, the corrugation deflects the incident trajectory, giving it a large momentum parallel to the surface and causing it to move quickly away from the adsorbate without reacting. The result is that the direct component of the reaction cross section (about half of the total) is actually less than the flat-surface value of 0.42 \AA^2 . However, the addition of the diffraction-mediated hot-atom channel leads to a total reaction cross section which is a bit larger than for a flat surface. Thus the parallel energy of the incident atom after impact and the competition between reaction and trapping remain useful concepts.

In Fig. 6 we plot a (two-dimensional) 2D ‘‘opacity function’’ $P_{\text{ref}}(x_i(0), y_i(0))$ for trajectories which reflect without reacting or trapping. For the area covered by the incident trajectories in Figs. 5 and 6, 77% of the trajectories trap without reacting, 22% reflect, and only about 1% react. Thus the ‘‘opacity’’ for trapping is roughly $1 - P_{\text{ref}}$. We plot the distribution for reflection, instead of trapping, because the structure is more apparent. While many of the trapped incident atoms have a positive total energy, $E_{\text{tot},i} > 0$, all trapped trajectories have a sizable residence time on the surface and can travel tens of \AA before being aborted. Examination of Fig. 6 shows that there is negligible reflection for ρ_0 less than about 2 \AA . At larger values of ρ_0 we begin to see the properties of the bare surface and a larger fraction of the incident atoms can reflect. Thus the influence of the adsorbate on trapping is quite large and almost every trajectory within 2 \AA of the adsorbed H either traps or reacts, as in the flat-surface case. The presence of the target atom not only adds a highly efficient mechanism for scattering and trapping the incident atom, but also acts to carry away some of its energy. For $\rho_0 \approx 0.2 \text{ \AA}$, the trapped incident atoms are bound in the z direction by about 1.7 eV , and $\langle E_{\text{tot},i} \rangle = -0.9 \text{ eV}$. Thus the target atom gains, on average, about 1 eV of energy. As ρ_0 increases, this energy transfer decreases to zero.

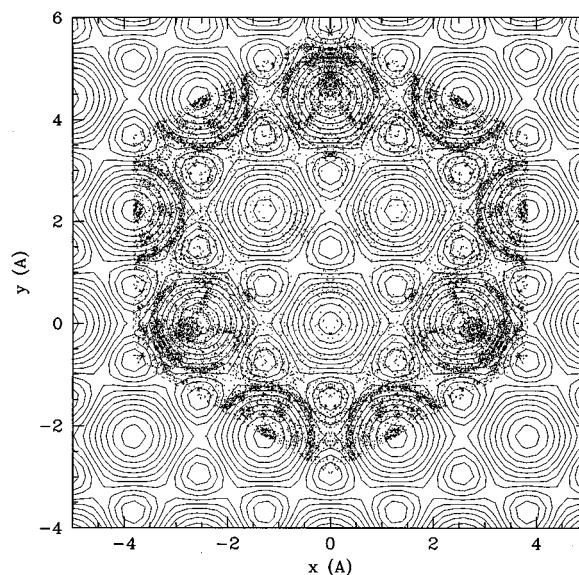


FIG. 6. Two-dimensional ‘‘opacity function,’’ $P_{\text{ref}}(x_i, y_i)$, for reflected trajectories, plotted as scattered points marking the initial values of x_i and y_i . The contours shown are for the corrugation function of the surface.

For $\rho_0 > 2.5 \text{ \AA}$ the target atom is relatively unperturbed and $\langle E_{\text{tot},i} \rangle$ is approximately the incident energy, $E_i = 75 \text{ meV}$. Thus interaction with the adsorbate can lead to true sticking ($\langle E_{\text{tot},i} \rangle < 0$), as well as an increase in trapping ($\langle E_{\text{tot},i} \rangle > 0$). Trapping at small ρ_0 leaves the target atom vibrationally excited and with enough lateral kinetic energy to occasionally escape from the hollow site, possibly reacting with another adsorbate. Eilmsteiner and Winkler¹⁴ have observed just this behavior in studies of H incident on D-covered Ni.

Our model only describes reactions with and scattering from a single adsorbate. At the high initial surface coverages of the experiments, the adsorbate–adsorbate spacing is $\approx 3 \text{ \AA}$ or more and the two trapping mechanisms should combine to trap a sizable percentage of the trajectories that do not undergo a direct ER reaction. Thus the reflection probability should be smaller than the single adsorbate value, more-or-less consistent with the experimental result of about 10%.⁸ It seems reasonable to conclude that a significant number of these trapped trajectories would eventually react at the high surface coverages of the experiments, and that trapping would be even more likely if coupling to the phonons was included. The total reaction cross section would then be on the order of several \AA^2 , in rough agreement with the experimental value. Our current model thus suggests that most of the reactions are hot-atom in nature. We should be careful, however, since earlier model PES’s gave us reaction cross sections as large as 2.4 \AA^2 . We are currently computing an improved PES and considering ways to model surface reactions involving several initially adsorbed species. Until then, however, we can get a rough description of these high-coverage hot-atom products by examining the large ρ_0 reactive trajectories in our current model.

We define a reaction time as the interval between the first turning point of the incident atom and the point where

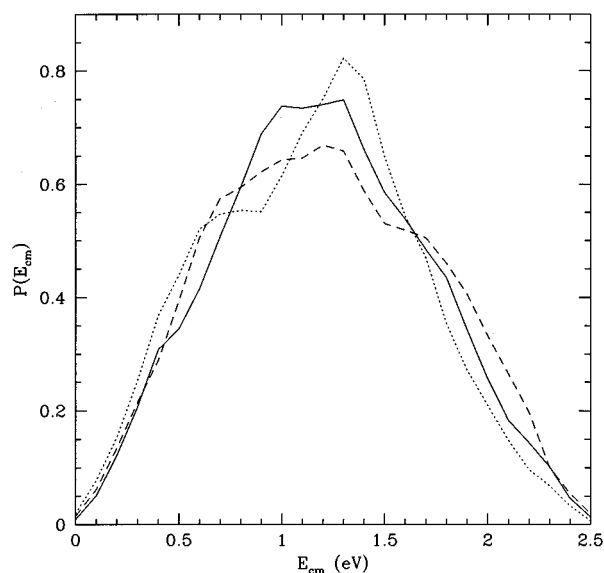


FIG. 7. Probability distribution for the product center-of-mass translational energy. H-on-H, straight line; H-on-D, dotted line; D-on-H, dashed line.

the molecular trajectory is stopped, 10.5 Å above the surface. For H₂, with 1.2 eV of translational energy normal to the surface (the average result), the flight time to the asymptotic region is ≈0.1 ps. For $\rho_0 \leq 1.2$ Å (direct or ER reactions) the average reaction time is about 0.1 ps, consistent with a direct mechanism. For $\rho_0 \geq 1.2$ Å (hot-atom region) the average reaction time varies between 0.3 and 0.6 ps, suggesting a surface residence time before reaction of about 0.2 to 0.5 ps. Given the low incident-to-metal atom mass ratio, the transfer of energy to the phonons is small for each collision with the surface and one might expect that surface residence times of several ps would be required for a significant dissipation of energy into the lattice.²⁵ Given the short residence times for these hot-atom reactions, we would expect only minor phonon effects, amounting to the loss of perhaps a few tenths of an eV to the lattice.

B. Product energy distributions

In Fig. 7 we plot the probability distribution for the product molecule center-of-mass translational energy, E_{cm} , for H-on-H, H-on-D, and D-on-H. In Fig. 8 we plot this energy averaged over trajectories with a given ρ_0 , $\langle E_{cm} \rangle(\rho_0)$, as a function of ρ_0 . We will plot several of our results in this fashion, to show how the different reaction pathways lead to different product behavior (see Fig. 4). Note that $\langle E_{cm} \rangle(\rho_0)$ should not be confused with $\langle E_{cm} \rangle$, the energy averaged over all reactive trajectories. For our incident energy of 75 meV, the total amount of energy available for the product degrees of freedom is about 2.5 eV for H-on-H and D-on-H, and a bit less for H-on-D, since D(ads) has a slightly smaller zero-point energy. A little less than half of this ends up in product translation, with $\langle E_{cm} \rangle = 1.2$ eV for all three isotopic combinations. By energy conservation, the average product internal energy $\langle E_{int} \rangle$ is about 1.3 eV for all cases. Note, however, that the distribution is

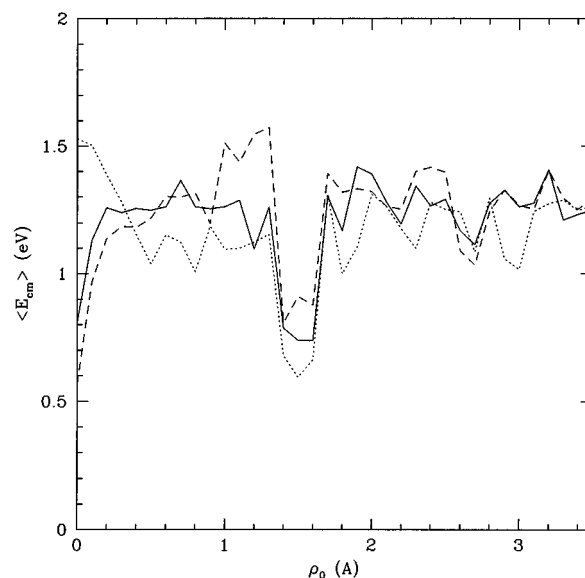


FIG. 8. Average product center-of-mass translational energy, as a function of the impact parameter, ρ_0 . H-on-H, straight line; H-on-D, dotted line; D-on-H, dashed line.

quite broad and many internal states and translational energies are possible. These averages are in excellent agreement with the experimental observations of Rettner and Auerbach,⁸ who measured $\langle E_{int} \rangle = 1.2$ and 1.3 eV for H-on-D and D-on-H, respectively. Thus there are minor isotope effects for these energies in both theory and experiment. For the flat-surface case, $\langle E_{cm} \rangle$ was a bit smaller, about 1.0 eV for H-on-H.

There is not much structure in the dependence of $\langle E_{cm} \rangle(\rho_0)$ and $\langle E_{int} \rangle(\rho_0)$ on ρ_0 , with two exceptions: $\rho \approx 0$ and 1.6 Å. Note that $\langle E_{int} \rangle(\rho_0)$ (not shown) is simply $2.5 \text{ eV} - \langle E_{cm} \rangle(\rho_0)$. The near zero impact collisions (except for H-on-D) result in a large internal energy. As can be seen in Fig. 9, where we plot the average product vibrational “quantum number,” $\langle \nu \rangle(\rho_0)$, as a function of ρ_0 , this energy is primarily in vibrational motion. This is similar to the flat-surface case, where the incident and adsorbed particles deflect away from one another after the initial impact, resulting in a large relative kinetic energy which becomes a large vibrational energy if the particles then leave the surface as a molecule. In fact, the rapid decrease of $\langle \nu \rangle(\rho_0)$ as ρ_0 increases from zero is consistent with our flat surface arguments. Note also that the dramatic increase of $\langle \nu \rangle(\rho_0)$ in the direct reaction region, as ρ_0 deviates from the minimum at $\rho_0 \approx r_0$, is consistent with the other opacity ideas discussed earlier.

The hot-atom reactions corresponding to $\rho_0 \approx 1.6$ Å also lead to an unusually large internal energy, which resides primarily in the vibrational degree of freedom. As discussed above, these trajectories also have a large relative kinetic energy, as the scattered incident particle moves towards the adsorbate through the bridge site. The hot-atom reactions at larger impact parameters exhibit much less vibrational excitation, and $\langle E_{cm} \rangle \approx \langle E_{int} \rangle \approx 1.25$ eV, independent of isotopic

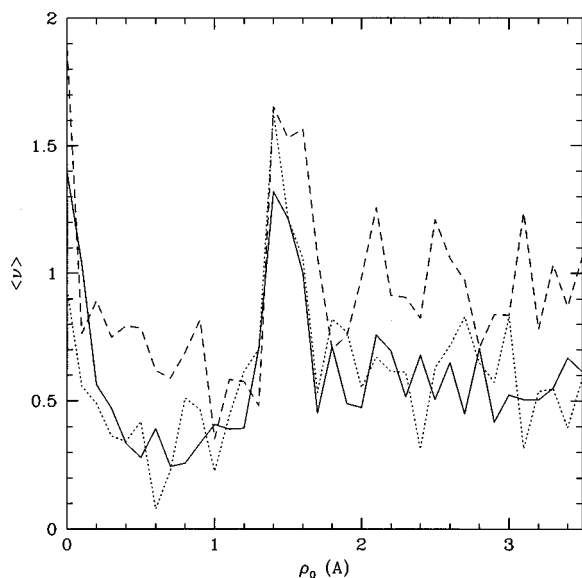


FIG. 9. Average product vibrational quantum number ν as a function of the impact parameter ρ_0 . H-on-H, straight line; H-on-D, dotted line; D-on-H, dashed line.

combination. This large ρ_0 result should be similar to that observed at high surface coverage, where hot-atom reactions dominate, and it is in excellent agreement with experiment.

As can be seen from Figs. 8 and 9, the dependence of $\langle E_{\text{int}} \rangle(\rho_0)$ on ρ_0 closely mirrors that of $\langle \nu \rangle(\rho_0)$ and, as one might surmise, there is not a strong variation of $\langle j \rangle(\rho_0)$ with ρ_0 (not plotted). For H-on-H, $\langle j \rangle$ varies between about 9 and 11 as a function of ρ_0 , with no simple dependence upon ρ_0 , except for a peak of $\langle j \rangle \approx 12$ for $\rho_0 = 1.6$ Å, and thus this pathway leads to slightly more rotational excitation. For the most part, there is little correlation between impact site and rotational excitation, in agreement with the flat-surface model.

In Figs. 10 and 11 we plot the vibrational and rotational product distributions, respectively, for three isotopic combinations. Note that given our definition of ν and the fact that classical mechanics does not respect zero-point energy, we can have $\nu = -1/2$. The averages $(\langle \nu \rangle, \langle j \rangle)$ are (0.59, 10.7), (0.59, 13.0), and (0.91, 11.7) for H-on-H, H-on-D, and D-on-H, respectively. Comparison with Table I shows that the basic trends are in agreement with experiment, except that the QC results for $\langle \nu \rangle$ and $\langle j \rangle$ are noticeably smaller and larger, respectively, than in the experiments. In both the theory and experiment, the isotope effects are small, with H-on-D leading to a bit less product vibration and a bit more product rotation than D-on-H. The discrepancy between theory and experiment with respect to the magnitude of $\langle \nu \rangle$ and $\langle j \rangle$ may have its origins in either the PES or errors from the use of classical trajectories. From Fig. 2 and Table I it is clear that the QC method, for the flat-surface case, generally underestimates $\langle \nu \rangle$ and overestimates $\langle j \rangle$, when compared with exact quantum results. Thus a quantum calculation may give a better agreement with experiment.

For H-on-D and D-on-H the reaction cross sections are

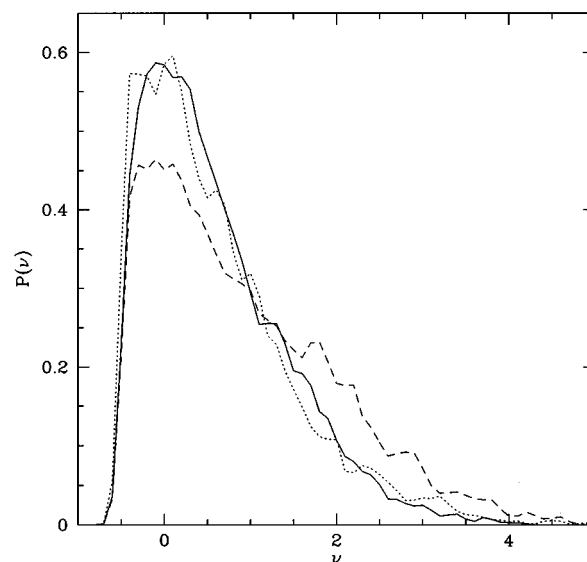


FIG. 10. Vibrational product distribution. H-on-H, straight line; H-on-D, dotted line; D-on-H, dashed line.

0.46 and 0.56 \AA^2 , respectively. Assuming our PES and QC cross sections are reasonably accurate, most of the products observed in the experiments must originate from hot-atom reactions, and we can estimate their behavior from our data in the large ρ_0 region. Note, however, that $\langle \nu \rangle(\rho_0)$ at large ρ_0 is about the same as $\langle \nu \rangle$ and, in our current model, both the direct and hot-atom product distributions are more-or-less consistent with experiment.

It is interesting to apply some very crude statistical ideas to the distribution of energy among the product degrees of freedom. If one puts an amount of energy $kT/2$ into each quadratic degree of freedom of the product molecule, $3kT/2$ goes into translation and kT goes into both rotation and vi-

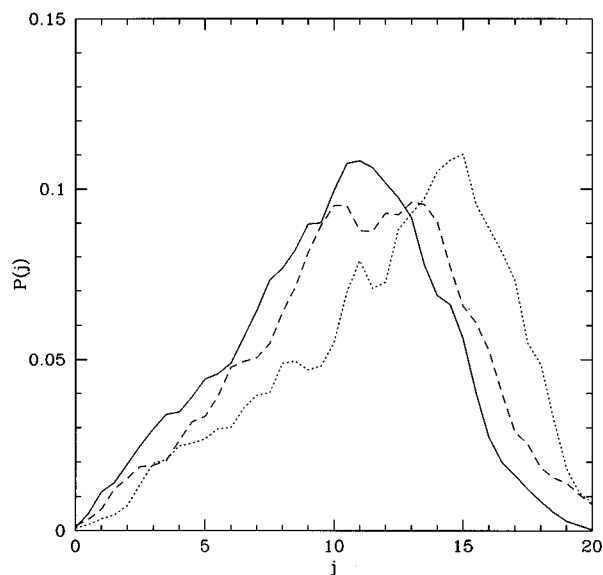


FIG. 11. Rotational product distribution. H-on-H, straight line; H-on-D, dotted line; D-on-H, dashed line.

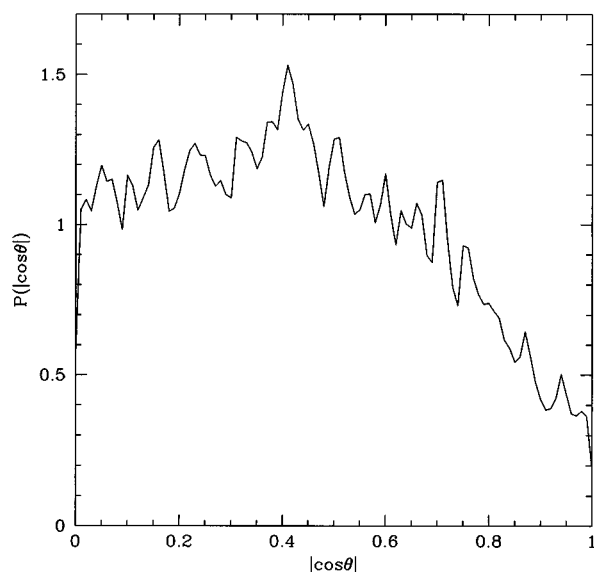


FIG. 12. Probability distribution for $|\cos \theta| = |J_z|/J$, for product H_2 molecules.

bration, in the harmonic approximation. If the total $7kT/2$ is set equal to the total available energy of 2.5 eV, we find that $\langle E_{\text{cm}} \rangle = 1.1$ eV, $\langle E_{\text{int}} \rangle = 1.4$ eV, $\langle \nu \rangle = 0.8$, and $\langle j \rangle = 9.8$. While these values are only in rough agreement with the theoretical and experimental results, they suggest that the reaction pathways may be quite complex, involving many collisions and a randomization of the energy, resulting in small isotope effects.

In an earlier work²² we discussed the possibility that hot-atom reactions, since they took place in the plane of the surface, might lead to products that rotated preferentially parallel to the surface plane. That is, their angular momentum vectors would be normal to the surface (helicopters). A direct reaction, on the other hand, may lead preferentially to molecules with their angular momentum vectors parallel to the surface (cartwheels), particularly at the near-normal incidence conditions in the experiments. Note that for a flat surface and normal incidence, the resulting products all result from direct reactions and all are rigorously $J_z = 0$ (cartwheels), where J_z is the z component of the angular momentum. In Fig. 12 we plot the probability distribution for $|\cos \theta| = |J_z|/J$, where θ is the angle between the angular momentum vector and the surface normal. $P(|\cos \theta|)$ is fairly flat, then drops off for $|\cos \theta| \geq 0.5$. We thus get less helicopter-type motion ($\theta = 0, \pi$) than cartwheel behavior. In Fig. 13 we examine $\langle |\cos \theta| \rangle(\rho_0)$ as a function of ρ_0 . At small ρ_0 (direct ER region) there is a tendency to favor cartwheel motion, but not a strong tendency. Thus the corrugation, which eliminates conservation of J_z , has a sizable effect. At larger ρ_0 (hot-atom region) we see more helicopters, but not a preponderance. In fact, neither orientation is favored and the trajectories leading to hot-atom reactions can be complicated. The hot atoms have a sizable energy normal to the surface, and can oscillate in that direction with an amplitude of an Å or more as they move about the surface.

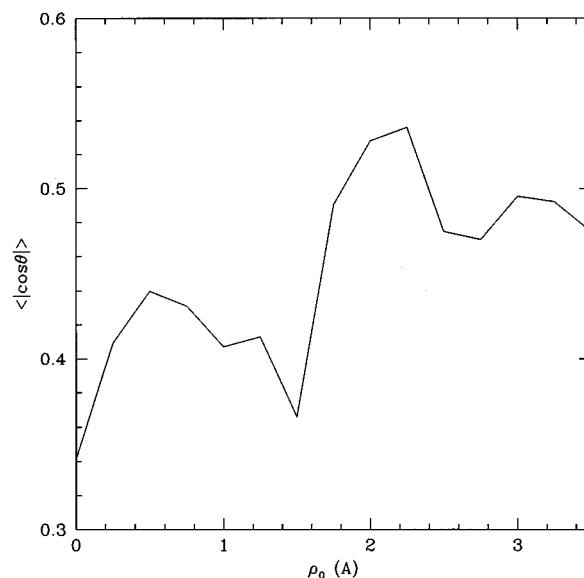


FIG. 13. Average of $|\cos \theta| = |J_z|/J$ as a function of the impact parameter ρ_0 .

Thus the resulting reaction dynamics do not necessarily take place in the plane of the surface. In a recent classical study of $\text{H}(\text{g}) + \text{H}/\text{Si}$ Eley–Rideal reactions, Kratzer³² has seen a tendency for direct reactions to favor cartwheel-type motion, as we do. However, unlike our study, he sees a tendency for hot-atom reactions to lead to helicopter motion. In the Kratzer study, however, the hot-atom channel resulted from the incident atom scattering from an adsorbate and reacting immediately with a neighboring adsorbate, which is much different from the hot-atom channel explored in our study.

In order to examine more closely some of our flat-surface ideas, we plot in Fig. 14 the average relative kinetic energy of the two particles, $\langle K_{\text{rel}} \rangle(\rho_0)$, at the time of the first turning point of the incident atom, for both reactive and trapped trajectories, as a function of ρ_0 . For the trapped trajectories at very small ρ_0 , $\langle K_{\text{rel}} \rangle(\rho_0)$ is large, due to the adsorbate-mediated trapping mechanism, and decreases rapidly with ρ_0 , as in the flat-surface case. For $\rho_0 \geq 0.3$ Å, $\langle K_{\text{rel}} \rangle(\rho_0)$ increases due to corrugation effects. As ρ_0 continues to increase, $\langle K_{\text{rel}} \rangle(\rho_0)$ drops to a small value of about 0.1 eV, corresponding to scattering from the bare surface corrugation. This transfer of energy from normal to parallel motion is smaller at large ρ_0 but is sufficient for trapping since the asymptotic normal translational energy is small, in both our simulations and the experiment. As seen earlier, the presence of the adsorbate strongly increases this energy transfer, and the trapping efficiency. The similar masses of the incident and adsorbed atom and the loosely bound nature of the adsorbate parallel to the surface makes the energy transfer efficient and the effects appear to be so long range as to make it difficult to decouple the adsorbate- and corrugation-mediated trapping mechanisms.

For reactive trajectories, we do not see this kind of structure. There is not a correlation between the relative energy of the particles and the final vibrational state of the product, as

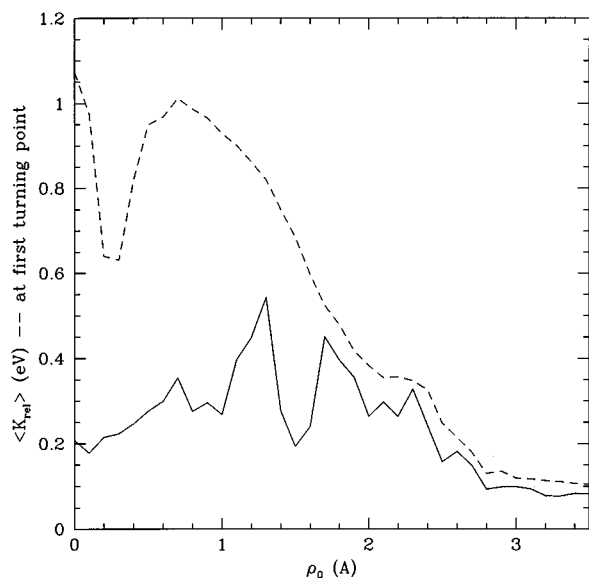


FIG. 14. Average relative kinetic energy K_{rel} for relative motion of the two bodies parallel to the surface, as a function of the impact parameter ρ_0 , computed at the first turning point of the incident atom. The straight line refers to trajectories that eventually lead to reaction; the dashed line refers to trajectories that eventually lead to trapping.

for a flat surface. However, the competition between trapping and reaction remains a very important concept. In the direct ER reaction region, those trajectories which have a large K_{rel} , due to interactions with the corrugation or the adsorbate, go on to trap without reacting. Only when K_{rel} is small do we see direct reaction, as in the flat-surface case. Note that the dip in $\langle K_{\text{rel}} \rangle(\rho_0)$ at $\rho_0 \approx 0.3 \text{ \AA}$ (for trajectories which trap) corresponds to the main peak in reactivity in Fig. 4.

V. SUMMARY

In conclusion, we have reexamined our quantum and classical flat-surface studies of $\text{H}(\text{g}) + \text{H}/\text{Cu}$ Eley–Rideal reactions in terms of opacity ideas and the competition between trapping and reaction. A modified potential energy surface that includes the effects of surface corrugation has been constructed from density functional studies of the interaction between H and a Cu(111) surface. Full six-degree-of-freedom quasiclassical studies were made of the reaction between an H atom entering from the gas phase and an H atom adsorbed on the hollow site of Cu(111). Several interesting observations can be made.

Adsorbate-mediated and corrugation-mediated trapping of the incident particle are both highly efficient and as such they compete strongly with reaction for the total cross section. For all trajectories incident within 2 \AA of the adsorbate, the two mechanisms combine to make trapping highly probable.

The addition of corrugation decreases the direct ER reaction cross section by deflecting away atoms which are incident on the surface more than a few tenths of an Å away from the adsorbate (towards the atop sites). Most of the di-

rect reactions thus result from trajectories incident very near the adsorbate hollow or the neighboring bridge sites, where deflection by the corrugation is smaller. However, the presence of corrugation increases the total reaction cross section by adding a hot-atom reaction pathway. For a single surface adsorbate, the direct and hot-atom pathways each contribute about half to a total reaction cross section of 0.57 \AA^2 .

The trapped atoms have a sizable residence time on the surface, which should only increase with the addition of phonon dissipation effects. Thus at the high surface coverages of the experiments, a sizable percentage of the trapped trajectories will result in an eventual hot-atom reaction. The resulting reaction cross section would then be on the order of the surface unit cell area, perhaps several Å^2 , which is consistent with experiment. Thus given our approximate PES and the errors inherent in the assumption of classical dynamics, we would conclude that the bulk of the reactions are of the hot-atom variety, resulting from adsorbate mediated and corrugation mediated trapping. Typical hot-atom reaction times appear to be about $0.2\text{--}0.5 \text{ ps}$, and thus only a small part of the excess energy would be dissipated into the phonons.²⁵ Thus $\approx 80\text{--}90\%$ of the total exothermicity should show up in the products, making them appear to be (direct) Eley–Rideal.

Product rotational, vibrational, and translational energy distributions show some interesting correlation to surface impact site. Vibrational excitation for direct reactions appears to increase for impact parameters which are greater or less than the product equilibrium bond length. The weak isotopic trends seen in the experiments are reproduced in both the direct and hot-atom channels of the QC calculation. While the computed product internal and translational energies were in excellent agreement with experiment, the QC results tended to give too little vibrational excitation and too much rotational excitation, compared with the experiments. Earlier calculations assuming a flat surface found the same relationship between the quantum and QC results, suggesting a better agreement might be found between experiment and a full six-degree-of-freedom quantum calculation.

In some earlier studies we suggested that direct reactions at normal or near normal incidence might lead to product molecules which exhibit predominantly “cartwheel” type motion, while hot-atom reactions in the surface plane should lead predominantly to “helicopters.” We observe a slight tendency towards “cartwheel” motion in the direct region, with no orientation favored in the hot-atom case. The corrugation effectively removes the $\Delta J_z = 0$ selection rule, leading to noncartwheel motion. As the hot adatoms bounce across the surface, they can be quite far above the surface plane because of their large energy normal to the surface, and reactions between these hot-atoms and the adsorbates do not generally occur in the surface plane.

The relative kinetic energy of the two particles immediately after their initial encounter is a useful idea for analyzing the results. This relative energy arises from the incident atom-adsorbate interaction or the incident atom-corrugation interaction and is sensitive to impact site. When this relative energy is large, the atoms separate too quickly to react and

trapping is highly efficient. In general, the competition between reaction and trapping should be an important concept in gas-adsorbate reactions.

Density functional methods are currently being used to explore the H–H interaction in the presence of the surface, in order to construct an improved PES. We have seen that the direct reaction cross section can be sensitive to certain regions of the PES²² and we are examining those regions. Given this, we should be able to provide a more accurate description of these Eley–Rideal reactions. We are also looking at the case of higher coverage and exploring the hot-atom reactions in more detail.

ACKNOWLEDGMENTS

S.C. and B.J. gratefully acknowledge support from the Division of Chemical Sciences, Office of Basic Energy Sciences, Office of Energy Research, U.S. Department of Energy, under Grant No. DE-FG02-87ER13744. M.P. is grateful for support by the Swedish Natural Science Research Council (NFR). Allocation of computer resources at the Center for Parallel Computers (PDC) is gratefully acknowledged.

- ¹R. I. Hall, I. Cadez, M. Landau, F. Pichou, and C. Schermann, *Phys. Rev. Lett.* **60**, 337 (1988).
- ²C. J. Eenshuistra, J. H. M. Bonnie, J. Los, and H. J. Hopmann, *Phys. Rev. Lett.* **60**, 341 (1988).
- ³K. R. Lykke and B. D. Kay, in *Laser Photoionization and Desorption Surface Analysis Techniques*, edited by N. S. Nogar [SPE **1208**, 18 (1990)].
- ⁴E. W. Kuipers, A. Vardi, A. Danon, and A. Amirav, *Phys. Rev. Lett.* **66**, 116 (1991).
- ⁵C. T. Rettner, *Phys. Rev. Lett.* **69**, 383 (1992).
- ⁶C. T. Rettner and D. J. Auerbach, *Science* **263**, 365 (1994).
- ⁷C. T. Rettner, *J. Chem. Phys.* **101**, 1529 (1994).
- ⁸C. T. Rettner and D. J. Auerbach, *Phys. Rev. Lett.* **74**, 4551 (1995); *J. Chem. Phys.* **104**, 2732 (1996).
- ⁹D. D. Koleske, S. M. Gates, and J. A. Schultz, *J. Chem. Phys.* **99**, 5619 (1993).
- ¹⁰D. D. Koleske, S. M. Gates, and B. Jackson, *J. Chem. Phys.* **101**, 3301 (1994).
- ¹¹C. C. Cheng, S. R. Lucas, H. Gutleben, W. J. Choyke, and J. T. Yates, Jr., *J. Am. Chem. Soc.* **114**, 1429 (1992).
- ¹²S. A. Buntin, *J. Chem. Phys.* **105**, 2066 (1996).
- ¹³T. A. Jachimowski and W. H. Weinberg, *J. Chem. Phys.* **101**, 10997 (1994).
- ¹⁴G. Eilmsteiner, W. Walkner, and A. Winkler, *Surf. Sci.* **352-354**, 263 (1996); G. Eilmsteiner and A. Winkler, *ibid.* **366**, L750 (1996).
- ¹⁵M. Xi and B. E. Bent, *J. Chem. Phys.* **97**, 4167 (1993); C. Lutterloh, J. Biener, A. Schenk, and J. Küppers, *Surf. Sci.* **331-333**, 261 (1995); *J. Chem. Phys.* **104**, 2392 (1996); J. Biener, C. Lutterloh, A. Schenk, K. Pöhlmann, and J. Küppers, *Surf. Sci.* **365**, 255 (1996); Y.-S. Park, J.-Y. Kim, and J. Lee, *ibid.* **363**, 62 (1996).
- ¹⁶J. B. U. A. Schubert, A. Schenk, B. Winter, C. Lutterloh, and J. Küppers, *J. Chem. Phys.* **99**, 3125 (1993); C. Lutterloh, A. Schenk, J. Biener, B. Winter, and J. Küppers, *Surf. Sci.* **316**, L1039 (1994); B. D. Thomas, J. J. N. Russel, P. E. Pehrsson, and J. Butler, *J. Chem. Phys.* **100**, 8425 (1994).
- ¹⁷C. T. Rettner, D. J. Auerbach, and J. Lee, *J. Chem. Phys.* **105**, 10115 (1996).
- ¹⁸B. Jackson and M. Persson, *J. Chem. Phys.* **96**, 2378 (1992); *Surf. Sci.* **269/270**, 195 (1992).
- ¹⁹B. Jackson, M. Persson, and B. D. Kay, *J. Chem. Phys.* **100**, 7687 (1994).
- ²⁰M. Persson and B. Jackson, *J. Chem. Phys.* **102**, 1078 (1995).
- ²¹M. Persson and B. Jackson, *Chem. Phys. Lett.* **237**, 468 (1995).
- ²²B. Jackson and M. Persson, *J. Chem. Phys.* **103**, 6257 (1995).
- ²³B. Jackson and M. Persson, in *Elementary Processes in Excitations and Reactions on Solid Surfaces*, edited by A. Okiji, H. Kasai, and K. Makoshi, Springer Series in Solid-State Sciences, Vol. 121 (Springer-Verlag, Berlin, 1996).
- ²⁴J. Harris and B. Kasemo, *Surf. Sci.* **105**, L281 (1981).
- ²⁵J. Strömqvist, L. Bengtsson, M. Persson, and B. Hammer, *Surf. Sci.* (submitted).
- ²⁶R. D. Levine and R. B. Bernstein, *Molecular Reaction Dynamics and Chemical Reactivity* (Oxford University Press, New York, 1987).
- ²⁷This range of chemisorption energies is obtained from the observation that H adsorption is thermodynamically stable, and from the observed maximum internal energy of HD molecules formed by recombinative desorption of incident D(g) atoms with adsorbed H atoms. This matter is discussed in detail in Ref. 25.
- ²⁸C. L. Lamont, B. N. J. Persson, and G. P. Williams, *Chem. Phys. Lett.* **243**, 429 (1995).
- ²⁹T. R. Mattson, G. Wahnström, L. Bengtsson, and B. Hammer, *Phys. Rev. B* **56**, 2258 (1997).
- ³⁰See the separate contributions by B. E. Hayden and S. Holloway and H. A. Michelsen, C. T. Rettner, and D. J. Auerbach, in *Surface Reactions*, edited by R. J. Madix (Springer-Verlag, Berlin, 1993).
- ³¹B. Hammer, M. Scheffler, K. W. Jacobsen, and J. K. Nørskov, *Phys. Rev. Lett.* **73**, 1400 (1994).
- ³²P. Kratzer, *J. Chem. Phys.* **106**, 6752 (1997).